Residual Learning Diagnosis Detection: An Advanced Residual Learning Diagnosis Detection System for COVID-19 in Industrial Internet of Things

Mingdong Zhang, Ronghe Chu, Chaoyu Dong, Jianguo Wei, *Member, IEEE*, Wenhuan Lu, *Member, IEEE*, and Naixue Xiong, *Senior Member, IEEE*

***Abstract*—Due to the fast transmission speed and severe health damage, COVID-19 has attracted global attention. Early diagnosis and isolation are effective and imperative strategies for epidemic prevention and control. Most diagnostic methods for the COVID-19 is based on nucleic acid testing (NAT), which is expensive and time-consuming. To build an efficient and valid alternative of NAT, this article investigates the feasibility of employing computed tomography images of lungs as the diagnostic signals. Unlike normal lungs, parts of the lungs infected with the COVID-19 developed lesions, ground-glass opacity, and bronchiectasis became apparent. Through a public dataset, in this article, we propose an advanced residual learning diagnosis detection (RLDD) scheme for the COVID-19 technique, which is designed to distinguish positive COVID-19 cases from heterogeneous lung images. Besides the advantage of high diagnosis effectiveness, the designed residual-based COVID-19 detection network can efficiently extract the lung features through small COVID-19 samples, which removes the pretraining requirement on other medical datasets. In the test set, we achieve an accuracy of 91.33%, a precision of 91.30%, and a recall of 90%. For the batch of 150 samples, the assessment time is only 4.7 s. Therefore, RLDD can be integrated into the application programming interface and embedded into the medical instrument to improve the detection efficiency of COVID-19.**

***Index Terms*—Computed tomography (CT) image analysis, convolutional neural network (CNN), COVID-19 diagnosis, industrial Internet of Things (IIoT), residual learning diagnosis detection (RLDD).**

NOMENCLATURE

NAT	Nucleic acid testing.
CT	Computed tomography.
RLDD	Residual learning diagnosis detection.
CNN	Convolutional neural network.
RT-PCR	Reverse transcription polymerase chain reaction.
P	Precision rate.
R	Recall rate.

I. INTRODUCTION

THE COVID-19 is breaking out worldwide. The fast spread of pneumonia virus causes more than three hundred thousand people to die all over the world. In the worst-affected areas, the number of dead and confirmed is still climbing.

People with COVID-19 generally have difficulties in breathing as well as rise of body temperature. During coronavirus incubation period, there could even be some asymptomatic infected persons in the population, which accelerates the spreading speed. Once infected, this virus would seriously damage people's health and safety. Therefore, timely and effective diagnosis and isolation of infected people are extremely necessary to prevent and relieve the epidemic diffusion. Currently, most hospitals diagnose the COVID-19 based on the reverse transcription polymerase chain reaction (RT-PCR) testing using a nasopharyngeal swab and the IgM antibody testing with a venous blood method. Both of them require contact between patients and doctors, which also takes around 24 h to get the results.

In [1], the chest computed tomographic (CT) scans of a 75-year-old male patient with severe COVID-19 were presented to show the early fibrosis. The effectiveness of ultrahigh-resolution CT was reported in [2] for the identification of lung abnormality. The clinical records and chest CT scans of 24 patients were analyzed in [3] for the transmission investigation. According to [1] and [3], the symptom of COVID-19 is closely related to the lung CT images. In the meantime, RNA detection is very time-consuming and expensive, which leads to the slow

Manuscript received September 21, 2020; revised December 9, 2020; accepted December 28, 2020. Date of publication January 15, 2021; date of current version June 16, 2021. This work was supported in part by the National Key Research and Development Program of China under Grant 2018YFC0806802, in part by the National Natural Science Foundation of China under Grant 61876131 and Grant U1936102, and in part by the Tianjin Key Project of AI under Grant 19ZXZNGX00030. Paper no. TII-20-4402. *(Corresponding authors: Chaoyu Dong; Jianguo Wei.)*

Mingdong Zhang, Ronghe Chu, Jianguo Wei, and Wenhuan Lu are with the College of Intelligence and Computing, Tianjin University, Tianjin 300072, China (e-mail: zhangmd@tju.edu.cn; chu_rh@tju.edu.cn; jianguo@tju.edu.cn; wenhuan@tju.edu.cn).

Chaoyu Dong is with the Nanyang Technological University, Singapore 639798, Singapore (e-mail: dong_chaoyu@ntu.edu.sg).

Naixue Xiong is with the Department of Mathematics and Computer Science, Northeastern State University, Tahlequah, OK 74464 USA (e-mail: xiongnaixue@gmail.com).

Color versions of one or more figures in this article are available at https://doi.org/10.1109/TII.2021.3051952.

Digital Object Identifier 10.1109/TII.2021.3051952

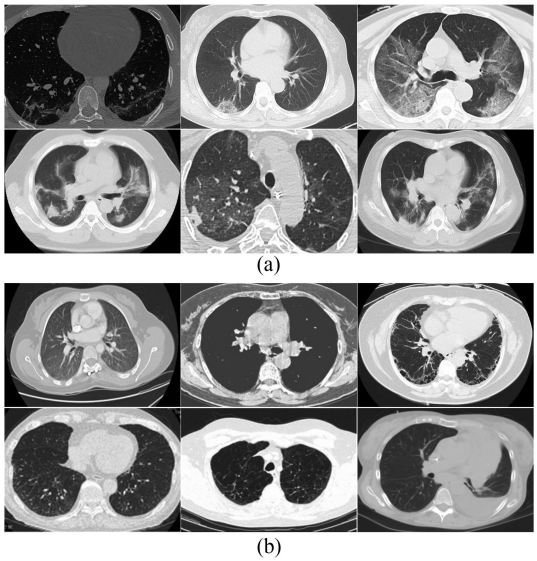

Fig. 1. Lung CT samples in the dataset. (a) Positive COVID-19. (b) Negative COVID-19.

detection of COVID-19 patients. On account of these two factors, an intelligent and efficient COVID-19 diagnosis strategy is developed in this article.

CT is a computed tomography without overlap. From [1] and [3], it can be found that the main features of CT of COVID-19 are: small patchy shadows of multiple lungs, or interstitial changes, mainly in the extrapulmonary zone. In the early stage, small patch shadows, ground glass shadows, and small cords of the stroma appear. After that, the patchy shadows will develop into ground lung glass-like changes and infiltration shadows, as shown in Fig. 1(a). White lung can be observed in severe cases, as well as serious hypoxemia. More severe patients would suffer from substantial changes and pleural effusion. The normal lung CT images of Fig. 1(b) show that the textures of the two lungs are clear, without abnormal trend distribution. There was no exudation or space-occupying lesions in the lung parenchyma. The two thoraxes were not enlarged. The trachea and bronchus were unobstructed with strengthened blood vessels and clear fat gaps. No enlarged lymph nodes were seen in the mediastinum. As the infected lung CTs are different from normal ones, it is possible to judge whether personal health with the lung CT features.

With the boost from artificial intelligence, many fields have made unprecedented progress. Learning-based detection works are prevalent in the industry, such as detecting defects in raw solar cell electroluminescence images [4], multimodal intelligence for fault diagnosis [5], and a kernel-driven semisupervised learning for nonlinear fault classification in industrial processes [6]. These learning-based approaches learn the underlying knowledge from the dataset. Similarly, we can use the dataset to generate a deep learning strategy for the COVID-19 detection diagnosis.

The public dataset [7] was released. With the help of Internet of Things (IoT), more scanning images can be collected automatically online. It helps to increase the dataset volume and the algorithm development. This dataset contains 349 lung CT samples for positive COVID-19 and 347 samples for negative cases. It facilitates the research and development from the learning-based aspect in the COVID-19 diagnosis. Focusing on detecting symptoms of COVID-19, we proposed a residual COVID-19 detection method. Our method can extract valid discriminative features to distinguish normal and positive COVID-19 cases. The experimental results suggest that our residual learning diagnosis detection (RLDD) scheme has achieved an accuracy of 91.33%, a precision of 91.30%, and a recall of 90%.

At present, the Industrial Internet of Things, i.e., (IIoT), is boosting the industrial revolution. It is transforming manufacturing, energy, transportation, cities, health care, and other industries [8], [9]. There are two applications in IIoT. On the one hand, the IIoT helps the diagnosis system automatically collect the data of COVID-19. With the increased dataset, the training performance can be further improved. On the other hand, the IIoT benefits the remote diagnosis. Without seeing the patient face-to-face, the detection system can tell the positive cases and negative cases remotely. This noncontact diagnosis reduces the infection possibility. The latest COVID-19 relevant information can help to optimize the RLDD model, which greatly improves the efficiency and accuracy of diagnosis. Our approach embeds a set of traditional CT technology in the industrial chain of artificial intelligent technology, transforming the traditional industry to a new stage of intelligent COVID-19 investigation. Compared with the depth network with the same number of parameters, each layer of the residual network only needs to learn the residual of the previous layer; the convergence speed of the residual network training is faster. In order to achieve higher efficiency, the residual structure is adopted in our model.

Different from the work of HSMAWOA and other algorithms in the image segmentation problem [10], the proposed approach designs the diagnosis workflow for the COVID-19, which consists of the complete image processing and the residual learning. The input images can be automatically resized and learned by the RLDD network. The main advantages of this article are highlighted as follows.

1) We exploit the strength of both residual learning methods and the deep convolutional neural networks (CNNs) and propose an advanced diagnosis detection scheme for image COVID-19.
2) A complete workflow of RLDD is developed for the COVID-19 diagnosis, which designs the data preprocessing, residual block, model, and training guidance.
3) The investigation results present that the developed method is efficient and accurate. The designed method is integrated with CT imaging instruments, which improve the efficiency of diagnosis and has practical application value.
4) A policy of combining RLDD with IIoT technology is proposed, to form an industrial chain of COVID-19 diagnosis combining traditional and intelligent technologies to realize a new stage of diagnosis on a global scale.

The rest of this article is organized. In Section II, we summarize recent research progress on the COVID-19 diagnosis. After that, we elaborate on the diagnostic scheme with RLDD in this article, including data preprocessing, the establishment of model, and algorithm, and the specific implementation of

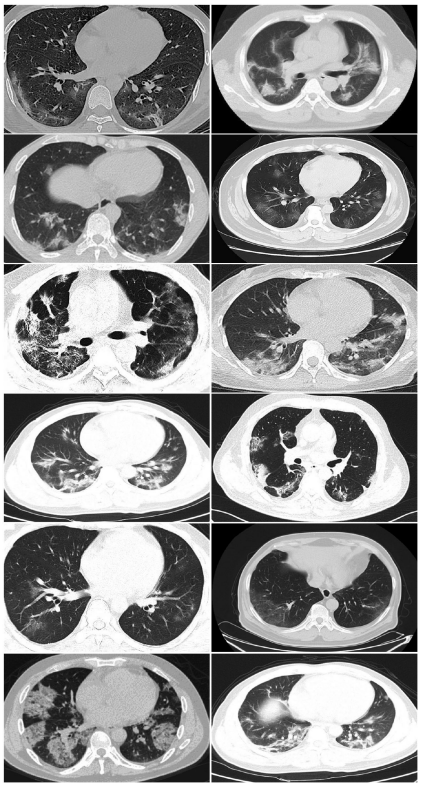

Fig. 2. CT scan samples of positive COVID-19 in dataset. The phenomenon of ground glass cloudy in the lungs and pleural effusion is obvious.

training methods Section III. In Section IV, we evaluated the diagnostic performance of the proposed RLDD scheme, and RLDD scheme has achieved an accuracy of 91.33%, a precision of 91.30%, and a recall of 90%. Finally, Section V concludes this article.

II. Related Research

A. Clinical Manifestations of COVID-19

In the CT images of Fig. 2, the feature of ground-glass opacity is initially used for the detection of symptomatic patient in the early period. [11]. There were small patchy shadows of multiple lungs and small cords of the stroma. After that, the patchy shadows will develop into ground lung glass-like changes and infiltration shadows [1],[3].

Besides, as an infectious lung disease, COVID-19 is accompanied by a series of side effects that include dry cough, fever, tiredness, shortness of breath, etc. [12]. Current studies have shown that sensory abnormalities are also related with COVID-19 cases. According to [13] and[14], researches claim that the loss of smell and taste are in higher possibility than fever and cough. It is consistent with the existing discovery that smell and taste are the better indicators of the virus.

B. COVID-19 Diagnosis Detection

Recently, the research [11] pointed out that the deployment of RT-PCR is common recently, accompanied with CT in the diagnosis of symptom staging. The work [11] reported that 36 were detected with SARS-CoV-2 among 51 persons. CT images are used as well as the swab-PCR test because of the false-negative rate during the PCR test. Similarly, recent studies show that as the RT-PCR is suffering from low sensitivity and low accuracy, repeated entries are required [15], [16]. Therefore, CT images combined with a computer-aided diagnosis for COVID-19 are necessary.

Furthermore, the intelligent diagnosis method based on deep learning COVID-19 has also made progress. The work [12] develops an end-to-end trainable deep few-shot with minimal training chest CT images for COVID-19 diagnosis detection. learning framework. Their model training processing contains the pretrain stage and the few-shot classification stage, and the result is remarkable. Unsupervised learning is one research branch in the machine learning area. The work [17] reviews one strategy with zero-shot learning for the COVID-19 diagnosis detection. The core techniques contain intermediate-space embedding, semantic embedding, visual embedding, and hybrid embedding models, which gives the method of transfer learning from the aspect of technology principle.

C. Algorithm Development

In the IIoT reliability diagnosis, image-based methodology is one of the major research topics. With the features extracted from available data, the long short-term memory (LSTM) network is used to build prediction models [18]. The advantage of the LSTM-based encoder–decoder architecture was demonstrated in various failure scenarios. Before the LSTM layer, the convolutional layers are employed to summarize the spatial information on the basis of images. Summarized hints of the individual images are provided by the convolution layers, which removes the redundancy due to neighboring pixels. The temporal network then extracts instant and periodic information from the low dimension. To deal with the high-dimensional problem, a separate deep autoencoder was also designed, which establishes the relationship between the individual image and a lower dimensional space.

Similarly, in the disease diagnosis, image-based methodology is an attractive field using abstract imaging characteristic to present the disease feature. With potential predictive power, the image-based diagnosis has important applications in personalized medicine. However, traditional models are afflicted by overfitting when a big variety of imaging features are at once considered in training and testing the predictive models [19]. Moreover, the diagnosis requires hand-crafted features that are not optimal to reduce bias. Although it is promising to assess medical images, images are usually valuated visually and qualitatively via physicians. However, the visual assessment and subjective description can suffer from a large disturbances. Hence, to quantify imaging essence, it is imperative for the disease diagnosis.

For the radiation images, the most common type is the deep CNN. By inheriting the properties from a general neural network, their specific features are also notable. A typical CNN comprises 20 layers, which could have more than 1000 layers [20]. Besides, the connected neurons make them possible to share multiple weights simultaneously. The advantageous structure makes the CNN effectively perform convolutions in face of

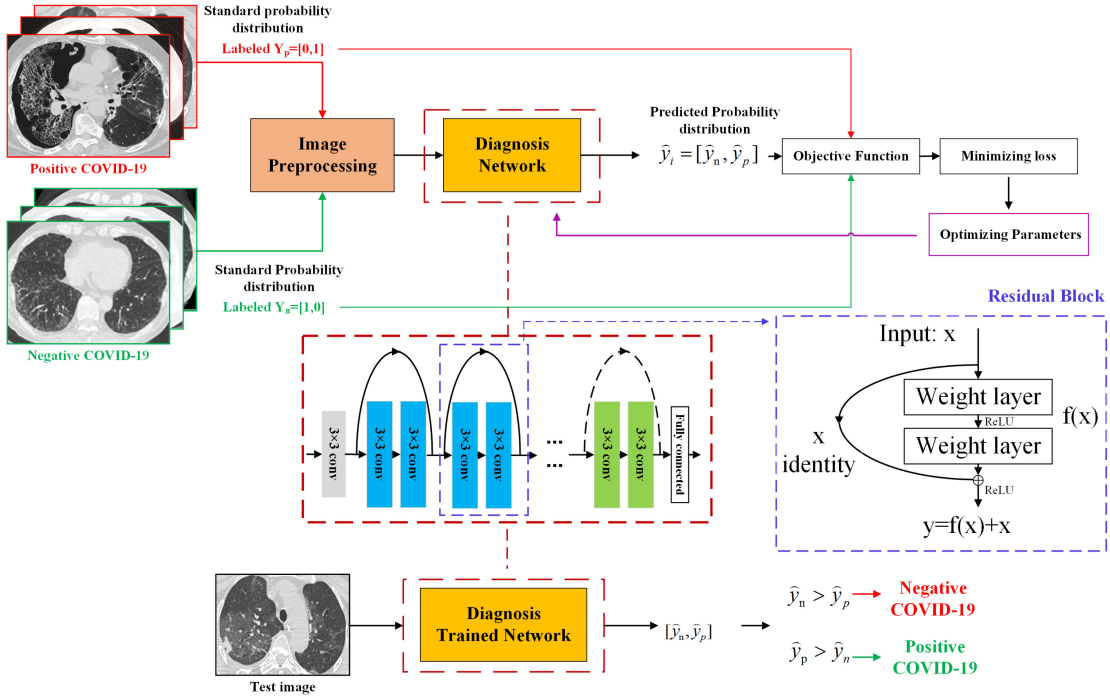

Fig. 3. Whole processing of our RLDD. First, the network is trained with tagged data. In the testing stage, we input the images to be tested into the network, calculate the probability of positive and negative, and give the diagnostic results.

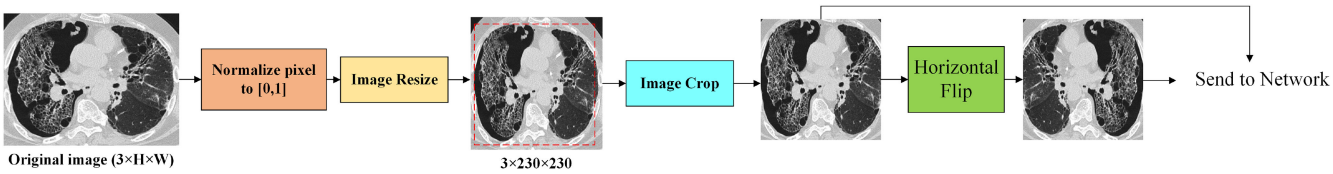

Fig. 4. Preprocessing design for CT images. The whole input computed tomographic image preprocessing process includes normalization, image resize, patch crop, and image horizontal flip enhancement.

the input images. Besides, between some layers, CNN performs pooling operations, making it robust to external changes in the dataset. Through different nonlinear transformations, the output is generated by the CNN. Because of the convenient structure, CNN can learn directly from training images and can be successfully applied for disease diagnosis and treatment planning. Despite CNNs being used for natural image analysis, the corresponding model has limited success in clinical applications, especially considering the current COVID-19 situation.

III. Our Proposed RLDD System

Facing the urgent requirement of fast diagnosis, an efficient neural network is developed to solve the pneumonia detection problem shown in Fig. 3. The specific details of our method are described in Sections II-A and II-B.

A. Data Preprocessing

According to the dataset [7], we learned that the shape of each CT image and the ratios of lung area in the image are different, as well as the unfixed position of the lungs in the image. Since the image resolution is not uniform and the dataset is not sufficient, the data preprocessing is necessary. The CT images are processed in RGB. To make the input image size consistent, uniform 224×224 image patches through resize and crop operation. Besides, the data is augmented by horizontal flip, random crop, and center crop operations to encourage the network to extract more effective features. After the image preprocessing, the training image size is $3 \times 224 \times 224$. The image preprocessing process is shown in Fig. 4. The probability of positive and negative COVID-19 are labeled y_p and y_n, respectively. The dataset is available at [Online]. Available: https://github.com/UCSD-AI4H/COVID-CT.

B. Residual Block

Our pneumonia detection network adopts the residual structure [21], which consists of residual blocks and dense layers in Fig. 5. The residual block in the red dotted box denotes the weight layer and nonlinearity as $f(\cdot)$, and the mapping of the residual block is:

$$y = f(\text{input}) + \text{input}, \tag{1}$$

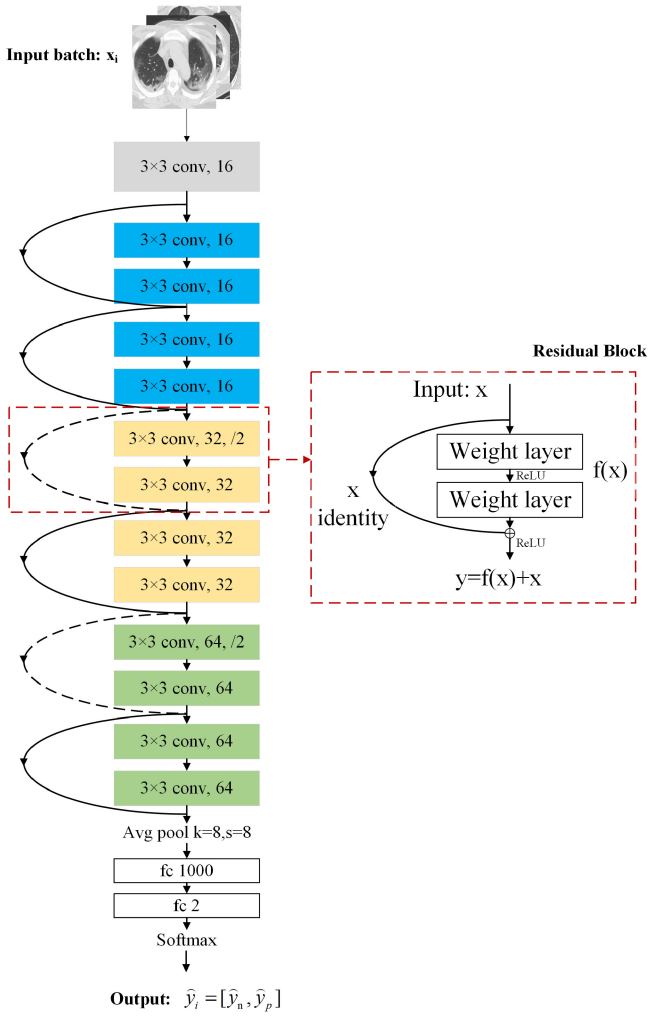

Fig. 5. Residual learning diagnosis detection convolutional neural network. The 3 × 3 conv and 32 represent the convolutional layer with a convolution kernel size of 3 × 3 with 32 convolution kernels; ReLU is used as the activation function. The fc represents the fully connected layer. The skip connection of the solid line represents add operation, while the skip connection of the dashed line unifies the channel dimensions and performs the additive operation.

where y is the output vectors on the basis of residual block. The operation is implemented through a shortcut link together with the elementwise addition. The nonlinear function $f(\cdot)$ presents the model complexity and fitting capability. When there are many redundant layers of stacked $f(\cdot)$ in-network, it is difficult for the network to learn identity mapping, which reduces the recognition accuracy of the network seriously. However, it is easier to push the residual $f(\cdot)$ to zero than to fit an identity mapping. With the shortcut connection, the $f(\cdot)$, the function $f(\cdot)$ only needs to learn the residual between y and x. When y is required to be equal to x in redundant layers, the residual function $f(\cdot)$ is pushed to zero. Therefore, the residual blocks can be used to build deep networks.

The residual-based pneumonia detection network in Fig. 5 contains six residual blocks, a fully connected layer, and an average pooling layer. The details of the residual block are shown in the red dotted box. Each rectangle represents a convolutional (conv) or a fully connected (fc) layer. Multiple residual layers are distinguished by different colors. Solid and dotted lines represent residual connections with the same size and different sizes. The k and s represent the kernel size and step size of the average pooling layer, respectively.

The entire figure shows our RLDD training process and testing process. Fig. 4 presents the whole process of RLDD. It mainly consists of two blocks: image preprocessing and diagnosis network. After the training, the RLDD network can be employed for the test images. We feed the preprocessed images into the convolutional network. During the training process, the network will extract the features of the original image and calculate the probability of each sample being positive and negative. We optimize the network parameters through the cross-entropy loss function. In the testing stage, we input the tested images to the network. The network calculates the probability of being positive and negative and gives the diagnostic results.

C. Model and Training

Our RLDD network contains 15 weight layers. To obtain a larger receptive field, the kernel size of our network is set to 3 × 3 [22]. Under the supervision training, the convolution layer learns to extract the crucial features that can be used to detect symptoms. Then, the combined characteristic from the last layer is sent to the pooling component and the dense neural network. Connecting to the network, the embedded softmax function transforms the fully connected layer into the probability distribution for classification between positive and negative situations. For the sample x_i, the predicted probability distribution is expressed as a vector $\hat{y_i}$

$$\begin{aligned}\hat{y_i} &= [\hat{y_{i-n}}, \hat{y_{i-p}}] \\ &= [(1-\hat{y_{i-p}}), \hat{y_{i-p}}], 0 \leq \hat{y_{i-p}}, \hat{y_{i-p}} \leq 1 \end{aligned} \tag{2}$$

where output $\hat{y_{i-p}}$ and $\hat{y_{i-n}}$ represent predicted positive and negative probabilities by network, respectively. The result of highest probability shows the diagnostic report. Formally, denoting the entire network mapping is $\mathcal{F}(\cdot;\theta)$. Therefore, output $[\hat{y_{i-n}}, \hat{y_{i-p}}]$ can be expressed as

$$[\hat{y_{i-n}}, \hat{y_{i-p}}] = \mathcal{F}(x_i;\theta). \tag{3}$$

Denoting the truth label of sample x_i is $y_i = [y_{i-n}, y_{i-p}]$. For a positive COVID-19 case, the truth label is $y_i = [0, 1]$ which represents the $y_{i-n} = 0$ and $y_{i-p} = 1$. The truth label for negative case is $y = [1, 0]$. Then, the cross-entropy loss function $L(x_i, y_i;\theta)$ is defined as the objective function of the network

$$\begin{aligned} L(x_i, y_i;\theta) &= -y_i \log \mathcal{F}(x_i;\theta) \\ &= -y_i \log \hat{y_i} \\ &= -[y_n, y_p] \log [\hat{y_{i-n}}, \hat{y_{i-p}}] \\ &= -y_p \cdot \log(\hat{y_{i-p}}) - y_n \cdot \log(\hat{y_{i-n}}). \end{aligned} \tag{4}$$

With the batch size N, its loss function will be

$$L(x, y;\theta) = \frac{1}{N} \sum_{i=1}^{N} (-y_p \cdot \log(\hat{y_{i-p}}) - y_n \cdot \log(\hat{y_{i-n}})). \tag{5}$$

By minimizing $L(x, y;\theta)$ in iteration, Adaptive moment estimation (Adam) algorithm [23] is introduced and utilized to

Algorithm 1: Residual Learning Diagnosis Detection Scheme for COVID-19.

Input: labeled dataset: $\{X, Y\}$
Output: optimal θ^*;
1: initial θ, epoch $= 0$, learning rate α
2: **repeat**
3: Sampling labeled data batch $\{x_i, y_i\}$ from $\{X, Y\}$
4: Performing forward propagation of the network and compute $[\hat{y_{i-n}}, \hat{y_{i-p}}]$
5: Compute loss L by (5)
6: Compute adaptive gradient by Adam: $\frac{\partial L}{\partial \theta} = \nabla_\theta \mathcal{F}(x_i; \theta)$
7: Update parameter $\theta \leftarrow \theta - \alpha \frac{\partial L}{\partial \theta}$
8: epoch $=$ epoch $+ 1$;
9: **until** (epoch $>$ Epochs)

accelerate pneumonia detection network convergence in training

$$\theta^* = \arg\min L(x, y). \tag{6}$$

With the convergence of network parameter values, the curve of loss function $L(x, y; \theta)$ tends to be smooth and stable, and the optimal weight parameters θ^* is obtained. The framework of the proposed RLDD scheme training step is outlined in Algorithm 1.

Different from [7], the proposed pneumonia detection network does not require the pretraining on other medical datasets, such as chest X-ray14 [24] in [7]. Limited by the fact that the dataset is not large enough, we allocate the training samples to 80%.

For process of the RLDD network, its batch size is set to 4. In Adam optimizer, the initial learning rate is 0.001, and the decay coefficient is 0.5. The number of epochs is specified as 1500. At the end of each epoch, the accuracy and average loss are calculated as shown in Fig. 6. During the training, it can be seen that the training loss function gradually decreases. The model accuracy on the training set finally reaches 99%. Since our network is a residual structure, this residual learning makes the feature extracted from each block be the residual feature of the previous block; so the convergence is faster. The training figures of each batch are generated by the rotation and crop. Each batch is different from others and introduces the training randomness, which leads to the spark during the training.

IV. Performance Analysis for COVID-19

A. Analysis of the Proposed Scheme

For the test process of RLDD, we first preprocessed the original CT image by cropping and resizing to facilitate the calculation of residual CNN. The image information of the training data is displayed in Table I. Then, we input the processed CT images into the CNN to infer a probability matrix, which represents the positive and negative probabilities of the input CT images. Finally, we take the class corresponding to the maximum probability value as the diagnostic result of RLDD.

Our test set contains 70 positive and 80 negative samples. The prediction results with the highest probability are employed as the diagnostic result of COVID-19. The prediction results are

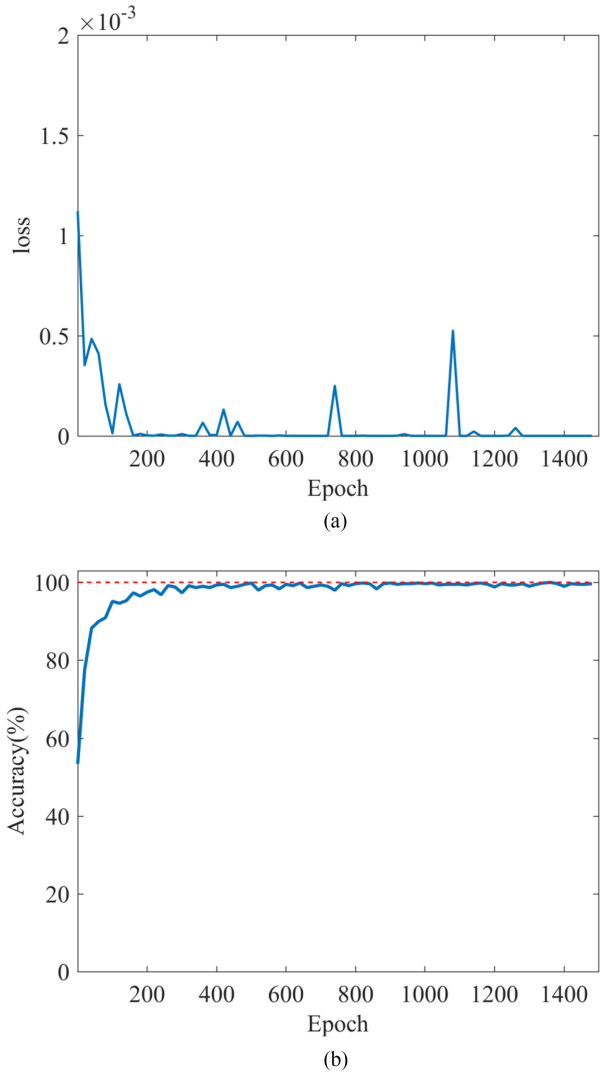

Fig. 6. Training curves. (a) Training loss curve. (b) Training accuracy curve. As the training progresses, the training loss function curve decreases gradually. During the training, we tested the accuracy of RLDD on the training set, which was recorded as (b). The accuracy converges to 99%, indicating that our model learning in the training set is close to saturation.

TABLE I
Parameters of Dataset and Neural Network

Maximum image	1637*1225
Minimum image	148*61
Resized image	224*224
Kernel size	3*3
Convolution kernel	32
Learning rate	0.001
Decay coefficient	0.5

listed in Table II. The accuracy rate, precision rate (P), recall rate (R), and $F1$ of the model are listed in Table III. The precision and recall are defined

$$P = \frac{\text{TP}}{(\text{TP} + \text{FP})} \tag{7}$$

TABLE II
PREDICTION RESULTS ON THE TEST SET. OUR TEST DATASET CONTAINS 150 SAMPLES, AND IT CONTAINS 70 CT IMAGE POSITIVE AND 80 NEGATIVE CT IMAGE SAMPLES

Label	Prediction Result	
	Positive	Negative
Positive	63	7
Negative	6	74

TABLE III
PERFORMANCE OF DEVELOPED METHOD IN THE TEST

Accuracy Rate	Precision Rate (P)	Recall Rate (R)	F1
91.33%	91.30%	90.00%	0.9065

TABLE IV
MODEL IS TRAINED AND TESTED ON FIVE SETS OF DATA, RESPECTIVELY

Number	Precision(P)	Recall(R)	F1	Accuracy Rate
1	89.71%	87.14%	0.8841	89.33%
2	89.86%	88.57%	0.8921	90.00%
3	92.42%	87.14%	0.8971	90.67%
4	91.04%	87.14%	0.8905	90.00%
5	90.91%	85.71%	0.8824	89.33%

$$R = \frac{\text{TP}}{(\text{TP} + \text{FN})} \tag{8}$$

where the number of true positive samples TP, negative samples TN, false positive samples FP, and false negative samples FN are denoted, respectively. The positive class indicates COVID-19 and negative class means normal case. The index $F1$ is expressed as follows:

$$F1 = \frac{(2 \times P \times R)}{(P + R)} \tag{9}$$

$$\text{acc} = \frac{\text{TP} + \text{TN}}{\text{sum}(\text{TP}, \text{FP}, \text{TN}, \text{FN})}. \tag{10}$$

To distinguish positive cases as soon as possible, high recall is imperative. Compared with [7], the recall rate is significantly improved compared with 76.2% in their paper. Meanwhile, the accuracy rate has a slight improvement. $F1$ is the harmonic mean of P and R, which indicates the developed model is more balanced and more practical.

Besides, our method supports simultaneous detection for large quantities of samples. It took 4.7 s to test 150 CT samples on GPU NVIDIA GTX 950 M. The time-consuming part is the CT images acquisition process, which takes half an hour on average. Influenced by medical resources, the current RT-PCR-based testing for COVID-19 can be as short as a few hours or as long as two days [25], especially in resource-poor settings. Our method has the advantage of timeliness in this respect.

To demonstrate that our diagnosis detection scheme is repeatable and not occasional, we construct a data-pool which contains all the data in the dataset. By using data-pool, we constructed training sets and test set five times. We trained the model in five training sets, and test the model in five corresponding test sets. From the summary in Table IV, we can learn that the diagnostic accuracy and recall of our model fluctuate around 90%, which is robust and not affected by data division. These rates are listed in Table IV, which is visualized in Fig. 7.

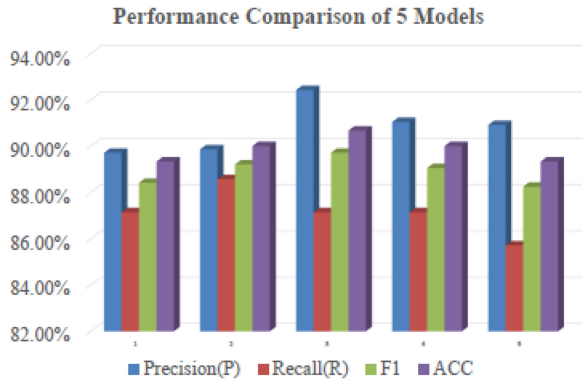

Fig. 7. Performance comparison of five models.

Finally, the visualized feature obtained by the network output is generated to understand the residual network has learned. In the last convolution layer, the kernel size is $64 \times 3 \times 3 \times 64$, and the feature map size is $N \times 64 \times 56 \times 56$. The 64 features of size 56×56 into an 8×8 block feature graph are shown in Fig. 5.

Each location in the feature map of the last convolutional layer contains different information of the original image, such as the outline of the image and information of the texture. The convolution layers map the original image from the spatial domain into the high-dimensional feature domain, which contains multiple spectral features of the original image. The full connection layer understands the high-dimensional feature and generates the prediction results. With a GPU of NVIDIA GeForce GTX 950 M, the assessment takes only 4.7 s for 150 CT samples, which notably accelerates the diagnosis process with the guarantee of high accuracy.

B. Practical Application

Because of the effectiveness, a feasible strategy is possibly established by applying the proposed method to practical application scenes. An application scene is given in Fig. 8. It shows the results of testing the performance of the five models. The distribution of histogram groups in the figure is similar, and various performance indexes of each model are similar. Therefore, the proposed diagnostic method is repeatable and not occasional.

In the doctor's office scenario, we installed the trained RLDD algorithm as an application program on the doctor.s computer terminal, which is shown in Fig. 9.

First, CT images of the patient's lungs are collected by the detector in the imaging acquisition room. Due to the influence of CT scanner itself and environment, the obtained image may be polluted by noise, very low resolution, too much white border, and other problems. Therefore, the image data cleaning process is essential and significant. For CT images with incomplete lung imaging or low resolution, we need to recollect them to ensure the images are clear and complete. For CT images with too many white borders, we should crop them and keep the original lung information of the image as much as possible. Then, the clean CT images are fed into the application program

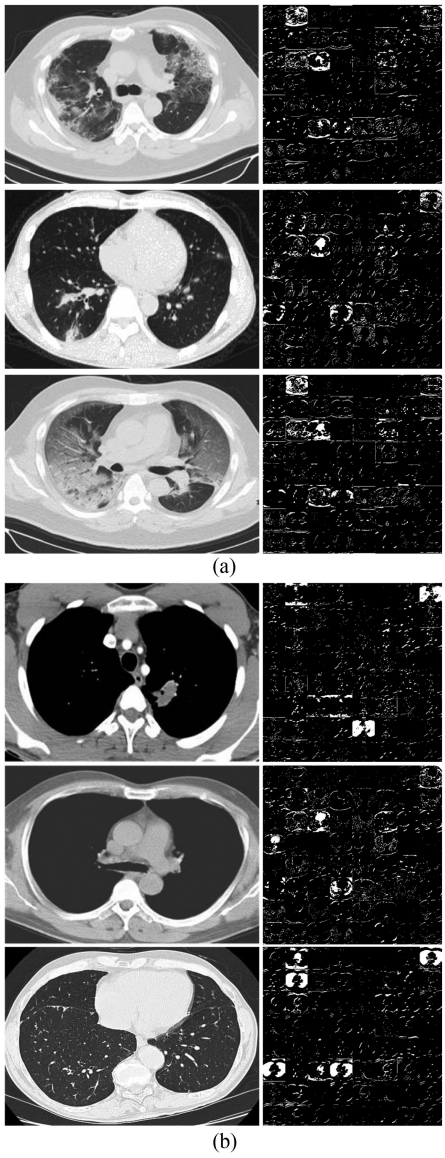

Fig. 8. Feature map extracted by network. Our RLDD can map the input CT image to features that contain key information of the original CT image, such as texture, edge, and potential feature encoding, which can be used to infer the positive or negative case of the input CT images. (a) Positive case. (b) Negative case.

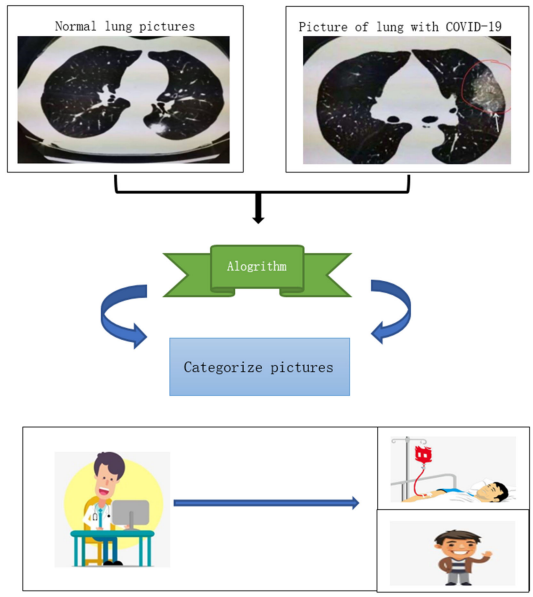

Fig. 9. Application of the proposed algorithm in detection of pulmonary symptoms of COVID-19.

Algorithm 2: Diagnostic Process of Practical Application and IIoT.

Output: The diagnosis: Positive or Negative;

1: Capture a CT image by computed tomography scanner.
2: Image preprocessing to ensure a complete and clear image.
3: Send the image to the application on the doctor's office computer.
4: Calculate the positive and negative probability of the test image, obtain $\hat{y_p}$, $\hat{y_n}$.
5: **if** $\hat{y_p} > \hat{y_n}$ **then**
6: The test case is predicted to be positive.
7: **else**
8: The test case is predicted to be negative.
9: **end if**
10: Tag the diagnostic results, upload labeled images to the server, and update the database.
11: Fine-tune the current model with new labeled images.
12: Optimize the model by integrating other diagnostic methods in the industry.

on the doctor's computer and are transmitted to the doctor's computer by the network. Our application program takes the received image as input and implement the forward propagation to obtain the prediction results. Finally, the cases confirmed by doctors are tagged and uploaded to the server to update database data in time. The new dataset is deployed to adjust the model. From this scenario, our RLDD has the following two advantages. 1) Face-to-face contacts between doctors and testers are not required, which reduces the chance of doctors being infected with COVID-19. 2) The proposed application can diagnose the CT image in a few seconds, and the doctor can get the diagnosis quickly so that a positive COVID-19 patient can get timely isolation and treatment. 3) Our applications have the potential to form a set of traditional CT technology to the industrial chain of artificial intelligent technology, with the advantages of short production cycle, high output and input ratio, and obvious future benefits.

V. Conclusion

This article proposed a RLDD scheme for COVID-19. By analyzing CT images, a difference was detected between the lungs with and without COVID-19, which supports the training of a convolutional neural network for the COVID-19 diagnosis. To avoid the gradient disappearance and impossibility, residual learning was utilized, specifically introducing residual blocks. The designed residual-based COVID-19 detection network can efficiently extract the lung differences between positive and negative samples, as well as the simplification of pretraining and

diagnosis processes. From demonstrated results, it showed that the RLDD is able to satisfy an accuracy of 91.33% and a recall rate of 90.0%, while the diagnosis efficiency is only 0.0313 s per sample.

Data have significant effect on the performance of neural networks with supervised learning. With the progress of the fight against COVID-19, relevant lung CT image data of various medical departments was accumulated. In future work, we will cooperate with key hospitals to expand our dataset so that the RLDD model can be trained more comprehensively. Thus, the detection performance and robustness of RLDD will be further improved. Besides, our followup work will introduce an attention mechanism for RLDD, which makes the convolutional layer focus on the main components, such as lung lobes, rather than the edges of the image. This technique will enable the network to extract more feature maps about the COVID-19 lesion area.

REFERENCES

[1] W. Zhang, "Imaging changes in severe COVID-19 pneumonia," *Intensive Care Med.*, vol. 46, no. 4, pp. 583–585, 2020.

[2] T. Iwasawa *et al.*, "Ultra-high-resolution computed tomography can demonstrate alveolar collapse in novel coronavirus (COVID-19) pneumonia," *Japanese J. Radiol.*, vol. 38, no. 5, pp. 394–398, 2020.

[3] Z. Hu, C. Song, C. Xu, G. Jin, and H. Shen, "Clinical characteristics of 24 asymptomatic infections with COVID-19 screened among close contacts in Nanjing, China," *SSRN Electron. J.*, vol. 63, no. 5, pp. 706–711, 2020.

[4] B. Su, H. Y. Chen, P. Chen, G. B. Bian, and W. Liu, "Deep learning-based solar-cell manufacturing defect detection with complementary attention network," *IEEE Trans. Ind. Informat.*, to be published, doi: 10.1109/TII.2020.3008021.

[5] Q. Zhang, C. Zhou, N. Xiong, Y. Qin, X. Li, and S. Huang, "Multimodel-based incident prediction and risk assessment in dynamic cybersecurity protection for industrial control systems," *IEEE Trans. Syst., Man, Cybern. Syst.*, vol. 46, no. 10, pp. 1429–1444, Oct. 2016.

[6] Z. Ge, S. Zhong, and Y. Zhang, "Semisupervised kernel learning for FDA model and its application for fault classification in industrial processes," *IEEE Trans. Ind. Informat.*, vol. 12, no. 4, pp. 1403–1411, Aug. 2016.

[7] J. Zhao, Y. Zhang, X. He, and P. Xie, "Covid-CT-dataset: A CT scan dataset about COVID-19," 2020. [Online]. Available: http://arxiv.org/abs/2003.13865.

[8] W. Wu, N. Xiong, and C. Wu, "Improved clustering algorithm based on energy consumption in wireless sensor networks," *IET Netw.*, vol. 6, no. 3, pp. 47–53, 2017.

[9] K. Huang, Q. Zhang, C. Zhou, N. Xiong, and Y. Qin, "An efficient intrusion detection approach for visual sensor networks based on traffic pattern learning," *IEEE Trans. Syst., Man, Cybern. Syst.*, vol. 47, no. 10, pp. 2704–2713, Oct. 2017.

[10] M. Abdel-Basset, V. Chang, and R. Mohamed, "Hsmawoa: A hybrid novel slime mould algorithm with whale optimization algorithm for tackling the image segmentation problem of chest x-ray images," *Appl. Soft Comput.*, vol. 95, 2020, Art. no. 106642.

[11] S. G. Chen, J. Y. Chen, Y. P. Yang, C. S. Chien, and L. T. Lin, "Use of radiographic features in COVID-19 diagnosis: Challenges and perspectives," *J. Chin. Med. Assoc.*, vol. 83, no. 7, pp. 644–647, 2020.

[12] X. Chen, L. Yao, T.Zhou, J.Dong, and Y. Zhang, "Momentum contrastive learning for few-shot COVID-19 diagnosis from chest CT images," *Pattern Recognit.*, vol. 113, pp. 1–8, 2021, Art. no. 107826.

[13] C. Menni, C. H. Sudre, C. J. Steves, S. Ourselin, and T. D. Spector, "Quantifying additional COVID-19 symptoms will save lives," *Lancet*, vol. 395, no. 10241, pp. e107–e108, 2020.

[14] C. Menni, A. M. Valdes, M. B. Freidin, C. H. Sudre, and T. D. Spector, "Real-time tracking of self-reported symptoms to predict potential COVID-19," *Nature Med.*, vol. 26, no. 7, pp. 1037–1040, 2020.

[15] T. Ai, Z. Yang, H. Hou, C. Zhan, and L. Xia, "Correlation of chest CT and RT-PCR testing in coronavirus disease 2019 (COVID-19) in China: A report of 1014 cases," *Radiology*, vol. 296, no. 2, pp. E32–E40, 2020.

[16] C. Long *et al.*, "Diagnosis of the coronavirus disease (COVID-19): RRT-PCR or CT?," *Eur. J. Radiol.*, vol. 126, 2020, Art. no. 108961.

[17] M. Rezaei and M. Shahidi, "Zero-shot learning and its applications from autonomous vehicles to COVID-19 diagnosis: A review," *SSRN Electron. J.*, vol. 3/4, pp. 1–21, 2020, Art. no. 100005.

[18] G. Aydemir and K. Paynabar, "Image-based prognostics using deep learning approach," *IEEE Trans. Ind. Informat.*, vol. 16, no. 9, pp. 5956–5964, Sep. 2020.

[19] S. S. Yip and H. J. Aerts, "Applications and limitations of radiomics," *Phys. Med. Biol.*, vol. 61, no. 13, 2016, Art. no. R150.

[20] M. A. Mazurowski, M. Buda, A. Saha, and M. R. Bashir, "Deep learning in radiology: An overview of the concepts and a survey of the state of the art with focus on MRI," *J. Magn. Reson. Imag.*, vol. 49, no. 4, pp. 939–954, 2019.

[21] K. He, X. Zhang, S. Ren, and S. Jian, "Deep residual learning for image recognition," in *Proc. IEEE Conf. Comput. Vis. Pattern Recognit.*, 2016, pp. 770–778.

[22] K. Simonyan and A. Zisserman, "Very deep convolutional networks for large-scale image recognition," *Comput. Sci.*, in *Proc. Int. Conf. Learn. Represent.*, 2015, pp. 1–14.

[23] D. Kingma and J. Ba, "Adam: A method for stochastic optimization," in *Proc. Int. Conf. Learn. Represent.*, 2014.

[24] X. Wang, Y. Peng, L. Lu, Z. Lu, M. Bagheri, and R. M. Summers, "Chestx-ray8: Hospital-scale chest x-ray database and benchmarks on weakly-supervised classification and localization of common thorax diseases," in *Proc. IEEE Conf. Comput. Vis. Pattern Recognit.*, 2017, pp. 3462–3471.

[25] N. J. Beeching, T. E. Fletcher, and M. B. J. Beadsworth, "Covid-19: Testing times," *Buried Multiple Junction*, vol. 369, 2020, Art. no. m1403.

Mingdong Zhang received the B.S. degree in software engineering from Tianjin University, Tianjin, China, in 2013.

His research interests include the application of artificial intelligence and deep learning.

Ronghe Chu received the B.S. degree in electrical engineering from the Tianjin University of Science and Technology, Tianjin, China, in 2019. He is currently working toward the M.S. degree in information and communication engineering with Tianjin University, Tianjin.

His research interests include machine learning, computer vision, and applied research.

Chaoyu Dong received the B.S. degree in electrical engineering from Tianjin University, Tianjin, China, in 2013.

His research interests include energy information system stability and artificial intelligence.

Jianguo Wei (Member, IEEE) received the B.S. degree in microelectronics from Jilin University in 1995, the M.S. degree in computer science and technology from Tianjin University in 2002, and the Ph.D. degree in computer science from the Japan Advanced Institute of Science and Technology (JAIST), Japan, in 2007.

He is currently a Professor with the College of Intelligence and Computing, Tianjin University. He has devoted himself to the research of speech signal processing, phonetics, and speech production.

Wenhuan Lu (Member, IEEE) received the master's degree in computer application from Tianjin University, China, in 2002, and the Ph.D. degree in artificial intelligence from the Japan Advanced Institute of Science and Technology (JAIST), Japan, in 2007.

She is currently an Associate Professor with the College of Intelligence and Computing, Tianjin University, China. She is working on speech security, personalized speech analysis with speech and language information processing technology applied to intelligent human-computer interaction system.

Naixue Xiong (Senior Member, IEEE) received the Ph.D. degrees in sensor system engineering and dependable sensor networks from Wuhan University, Wuhan, China, and Japan Advanced Institute of Science and Technology (JAIST), Nomi, Japan, in 2007 and 2008, respectively.

He has been a Professor with the College of Intelligence and Computing, Tianjin University, Tianjin, China, since 2017. His research interests include cloud computing, security and dependability, parallel and distributed computing, networks, and optimization theory.